*Korean J. Chem. Eng.*, 40(3), 630-641 (2023)
DOI: 10.1007/s11814-022-1249-2

pISSN: 0256-1115
eISSN: 1975-7220

# Cuprous oxide ($Cu_2O$) nanoparticles in nanofiltration membrane with enhanced separation performance and anti-fouling properties

**Abdolreza Moghadassi*,†, Shakiba Ghohyei*, Samaneh Bandehali*,†, Morteza Habibi**, and Maryam Eskandari***

*Department of Chemical Engineering, Arak University, Arak 38156-8-8349, Iran
**Department of Chemistry, Faculty of Science, Arak University, Arak 38156-8-8349, Iran
(*Received 4 May 2022 • Revised 23 July 2022 • Accepted 4 August 2022*)

**Abstract**−Cuprous oxide nanoparticles ($Cu_2O$) were synthesized by electrochemical method and as an add-on to construct polyethersulfone (PES) nanofiltration (NF) membranes. Field emission scanning electron microscopy (FESEM), 3D surface images, X-ray diffraction (XRD) analysis, and Fourier transform infrared (FTIR) spectroscopy were utilized to indicate membranes and nanoparticles. Membranes were evaluated by tests of water content, porosity, contact angle, salt rejection, water flux and average pore size measurements. The results show the enhancement of surface hydrophilicity by the addition of $Cu_2O$ nanoparticles. The highest unalloyed water flux was obtained by membrane, including 0.05 wt% $Cu_2O$ nanoparticles, and the highest rejection was revealed by a membrane containing 2 wt% $Cu_2O$ nanoparticles. The $Na_2SO_4$ rejection reached 66.94%, which was significantly higher than the bare PES membrane. This performance may be owing to increased $Na_2SO_4$ adsorption sites. The heavy metals rejection of $CrSO_4$, $Pb(NO_3)_2$, and Cu $(NO_3)_2$ increased 79.38%, 85.08%, and 81% for the M5 membrane, respectively, while it was 45%, 46%, and 49% for bare membrane, respectively. Furthermore, the flux of unalloyed water increased from 9.78 $L/m^2 \cdot h$ on the pure PES membrane to 36.78 $L/m^2 \cdot h$ on the M1 membrane. The decrease of surface roughness and also the increase of hydrophilic groups improved the antifouling properties of the membranes.

Keywords: Nanofiltration Membrane, Cuprous Oxide Nanoparticles, Salt Removal, Anti-fouling Properties

## INTRODUCTION

The nanofiltration (NF) process has made significant progress. Nanofiltration membranes are among the pressure-derived membranes due to their advantages compared to other separation methods [1-3], such as significant diffusion flux, low energy consumption, relatively low investment cost and unique separation capability for ions of dissimilar capacities [4-8]. NF membranes have been used at various stages of water and effluent treatment to remove microbial, chemical contaminants, and desalination [9-11]. Also, it has the capability for heavy metals, viruses, bacteria removal from water and wastewater. There are valuable new methods for the preparation of the copious-performance membrane and the modification of its properties, such as plasma treatment, adsorption, coating, surface grafting, and blending with different filler additives, and hydrophilic polymers [12-14]. The accession of nanoparticles into the polymer matrix results in high permeability, high selectivity, and improved properties like physicochemical properties. Metal oxide nanomaterials such as ZnO, CuO, $Cu_2O$, $Fe_2O_3$, $Al_2O_3$, and $TiO_2$ have unique chemical and physical properties due to their quantum size effect and wide effective surface area [15-19]. Copper oxide is two common forms of cuprous oxide ($Cu_2O$) and cupric oxide (CuO). The cupric oxide nanoparticles are semiconductor type-p with a monoclinic matrix structure, and cuprous oxide nanoparticles are semiconductor type-p with a cubic structure and a suitable direct bandgap (~2 eV) [20,21]. They have been used widely in solar cells, sensors (biosensors and gas sensors), polymer memory devices, semiconductor devices, lithium-ion batteries, and as a photocatalyst and electrocatalyst due to their better electrical conductivity, low growth temperature, and high catalytic activity [22,24].

$Cu_2O$ powder was used in this study as a modifier that can be manufactured by several methods, including thermal treatment [25], electrochemical [26], sonochemical [27], sol-gel, colloidal synthesis [28], electro-deposition [29], and thermal oxidation [30]. Kooti et al. [31] used an economical manner to synthesize $Cu_2O$ nanoparticles by diminution of the Fehling's solution (copper sulfate with potassium sodium tartrate in an alkaline), using glucose as reducing agent and sodium laureth sulfate (SLES) or Triton-X 100 as surfactants for control precipitation $Cu_2O$. As a result, they synthesized $Cu_2O$ nanoparticles with diameters of about 30 nm with high purity and almost quantitative yield in an inexpensive, effortless to control, reproducible and straightforward process. Valodkar et al. [32] investigated the formation mechanism of cuprous oxide ($Cu_2O$) dendrites in an easy hydrothermal direction using starch as a stabilizing agent and as reducing at two different temperatures. As result, spherical nanoparticles were obtained intrinsically at dendritic nanostructures of about 50 nm size at low thesis reaction temperatures. Khattar et al. [33] prepared $Cu_2O$ nanoparticles using an electrochemical cell comprising two compartments separated by a ceramic diaphragm. They used copper sheets as anode and cathode materials. The effect of sodium dodecyl sulfate (SDS), polyvinyl alco-

†To whom correspondence should be addressed.
E-mail: a-moghadassi@araku.ac.ir, s-bandehali@phd.araku.ac.ir

hol (PVA), glycerin, and KOH concentration on particle size and surface roughness was investigated: that its result was decreasing the roughness and particle size in less PVA amount. Figueroa et al. [34] produced cuprous oxide nanoparticles by electrochemical method with anodic disintegration of copper in an alkaline chloride sodium solution. The goal of this study was to establish a suitable measure for the production of industrially scale cuprous oxide nanoparticles using an anode support system.

After studying and researching to produce cuprous oxide nanoparticles with an optimum method, we finally concluded that the electrochemical method, due to the short production stages, easier operation, higher scale production, higher quality, cost-effectiveness, and easier operating conditions control, is more suitable for mass production among other methods [35-38].

In this research, the cuprous oxide ($Cu_2O$) nanoparticles were synthesized by electrochemical procedure using anodic disbandment of copper in an alkaline solution of sodium chloride and applied to fabricate NF membranes. Since, the hydrophilic properties and fouling resistance are the most significant achievements in NF membrane preparation. The composition system of nanoparticles and membrane provides a synergistic effect in water and wastewater treatment.

In García et al. [39], during the surface polymerization process, the composition of CuO nanoparticles in reverse osmosis composite membranes with a thin-walled was studied, which is a possible alternative to upgrade the bio-deposition capacity without disturbing membrane function. According to the literature, comparing the modified membrane with the pristine membrane, a higher roughness of the surface, similar contact angle and lower negative charge surface, and significant salt rejection were observed with stable water flux. Also, a fine anti-adhesion and antibacterial result were observed due to copper toxicity. In Zareei et al. [40], melange matrix prepared PES-based NF membranes via composite $CoFe_2O_4$/CuO nanoparticles, which by chemical precipitation method were synthesized. The flux recovery ratio, and pure water flux were measured. PES/$CoFe_2O_4$/CuO membrane at 0.5 wt% of nanoparticles demonstrated the increment of salts rejection of $Na_2SO_4$ and NaCl, and metal ions rejection of $Pb^{2+}$, $Ni^{2+}$, and $Cu^{2+}$ for the compounded membrane compared with the bare PES membrane. The mean surface roughness and water contact angle decreased. The surface hydrophilicity increased and the surface became smoother. The reusability survey for the transcendent mixed membrane appeared a scarce reduction in the median yield of less than 4.9%. From Singh et al. [41], polysulfone matrix ultrafiltration membranes were fabricated by introducing $Cu_2O$ photocatalyst nanoparticles. The antifouling nature was investigated by permeating BSA aqueous solutions, and hydrophilic qualities of modified membranes were studied through a comparison of the static water contact angle (SWCA). Drug elimination studies were performed using ibuprofen (IBP). Introducing $Cu_2O$ photocatalyst nanoparticles improves the membrane features, such as porosity, pore size distribution, and flux. These membranes revealed the decrease of SWCA, and the increase in the hydrophilicity of the membranes. Furthermore, BSA adsorption decreased and prosperous removal of IBP was accomplished at 86% under the evident light situation with a rate eradication of $32.63\times10^{-3}$ $min^{-1}$. Xu et al. [42] fabricated the blend membranes from polysulfone (PSf) and Ag-$Cu_2O$ nanowires (NWs) with outstanding antimicrobial performance through the phase inversion process, successfully. According to this research, the mixed membranes held a considerable antibacterial span with seldom liberating $Ag^+$. According to their results, compared to unalloyed PSf membrane, mixed membranes showed higher permeability, mainly when the Ag-$Cu_2O$ content of NWs was 0.5 wt%. Nasrollahi et al. [43] studied the impress of amine performance of ZnO and CuO nanoparticles as an additive on the permeation and the morphology qualities of PES nanocomposite ultrafiltration membranes. The increment of hydrophilicity and porosity of new membranes led to significant improvement of pure water flux and had a significant positive effect on permeability. Moreover, the obtained results revealed a good flux recovery ratio and antifouling properties.

Choudhury et al. [44] fabricated an innovative clay-alumina ceramic compound membrane inclusive of CuO nanoparticles and cellulose hydroxyethyl to separate Cr(VI) and Pb(II) from bedraggled water. In combination with biopolymer, addition of CuO nanoparticles causes an improvement of the heavy metal rejection rate. Moreover, the pore construction of macroporous ceramic lamella was upgraded from 0.5 to 1.5 μm to 3 nm.

Little attention has been paid to the use and modification of cuprous oxide nanoparticles ($Cu_2O$) in the preparation of membranes for water treatment. The present work investigates for the first time the use of cuprous oxide nanoparticles synthesized by electrochemical method for wastewater treatment. PES/$Cu_2O$ NF membranes were concocted per the phase inversion procedure. The PES in the groundwork of laboratory NF membranes is a hydrophobic polymer with good thermal durability and superior mechanical power [45]. The combined method, due to its inexpensiveness and its simpleness, is used in this perusal for the modification of PES membranes by introducing synthesized $Cu_2O$ nanoparticles as an additive. In this perusal, the infiltration of the $Cu_2O$ nanoparticles presence into the PES as a membrane matrix was studied on the separation performance and their physicochemical qualities. The ability of $Na_2SO_4$, $Cu(NO_3)_2$, $CrSO_4$ and $Pb(NO_3)_2$ removal from water solutions by membranes, antifouling property, its permeability, and separation performance were studied. The particle size and morphology of the synthesized nanoparticles were analyzed by analysis FTIR, XRD, and FESEM. Physicochemical qualities from concocted membranes were characterized by FESEM, FTIR, 3D surface images, and the measurements of porosity, contact angle, and water content.

## EXPERIMENTAL

### 1. Materials

Polyethersulfone (PES, $M_w$=58,000 g/mol) was provided by BASF, Germany, and polyvinylpyrrolidone (PVP, $M_w$=25,000 g/mol) as pore creating agent was provided by Merck, Germany. N, N-dimethylacetamide (DMAc (99.7%), $M_w$=87.12 g/mol) as solvent was prepared from Daejung, Korea. Sodium chloride, sodium hydroxide were provided from Dr. Mojallali Industrial Chemical Complex Company, Iran. In addition, the aqueous $CrSO_4$, $Na_2SO_4$, $Cu(NO_3)_2$, and $Pb(NO_3)_2$ solutions were provided from Merck, Germany, for membrane separation performance analysis.

**2. Synthesis and Specifications of $Cu_2O$ Nanoparticles**

The $Cu_2O$ nanoparticles were produced via electrochemical procedure with anodic disbandment of copper in an alkaline solution containing 250 g/l NaCl, 1 g/l NaOH and a polypropylene diaphragm to prevent moving $OH^-$ ions to the cathode. Also, the stainless steel sheet as cathode and copper electrode (99.9% Cu) as anode with dimensions (50 mm×56 mm) was applied. Electrolysis process done at operating conditions: temperature 81 °C, PH=10.1, C.d=2,000 A/m$^2$, for 30 minutes. Then deionized water was used for washing powders.

X-Ray diffraction analysis (XRD) was used to study the crystalline structure and size of $Cu_2O$ nanoparticles. The average size of cuprous oxide crystals (D) was evaluated using the Debye Scherrer equation in Eq. (1):

$$D_c \equiv \frac{k\lambda}{\beta\cos\theta} \tag{1}$$

where $\beta$ is the entire breadth at half maximum intensity of climax corresponding to $2\theta$ and K as a dimensionless value is equivalent to 0.9, and $\lambda$ is the X-ray wavelength.

Finally, Fourier transform infrared spectroscopy (FTIR), field emission scanning electron microscopy (FESEM), and mid a spectrometer Bruker (Tensor 27) were applied for verification of cuprous oxide nanoparticles formation.

**3. Manufacturing of NF Membranes**

Membranes were concocted through a phase inversion by submerging into a deionized water bath. The polymeric solutions from PVP (1 wt%) and PES (18%) in DMAc as a solvent with different amounts of $Cu_2O$ nanoparticles were prepared. Then casting solutions were stirred for 5 h at room temperature. Polymeric solutions were placed for 40 min in the ultrasonic bath for better dispersion of nanoparticles in the solution. The homogeneous solutions were conserved for 12 h without stirring at the same temperature due to detaching air bubbles. The polymer solutions were coated into a clean glass using a suitable applicator per a fixed thickness of 300 μm and then immediately doused in a deionized water bath. The prepared porous membranes were in deionized water for 24 h to remove water-soluble substances. They were placed between two paper filters to dry at room temperature. Table 1 shows the compositions of the casting solution.

**4. Characterization of Membranes**

FTIR analysis was applied to characterize $Cu_2O$ nanoparticles and prepared membranes. The spectra were recorded in a range of wavelengths from 500 to 4,000 cm$^{-1}$ with a perspicuity of 1 cm$^{-1}$ for each spectrum. The membrane surface morphology was analyzed with field emission scanning electron microscopy (FESEM, SU3500, USA). Before taking FESEM images, the prepared membranes were broken in liquid nitrogen and then smeared with gold to gain conductivity. Moreover, 3D surface images with a scanning area of 6 μm× 6 μm were exploited to specify the surface roughness of membranes by SPM software (version 6.4, Femtoscan).

The water contact angles ($\theta$) were assessed to survey the hydrophilicity of the surface membrane by using a contact angle measuring appliance. The probe liquid was deionized water. For decreasing experimental slips, the contact angle was assessed in three altered localities and their mean was related.

Water content was assessed by the diversity betwixt the withered and sodden weight of membranes. To measure the weight of wet membranes, the arranged membranes were in distilled water for 24 h then weighed. Wet membranes were dehumidified in an oven to achieve an immovable weight. The following equation was used to compute the water content:

$$\text{Water content}\ (\%) \equiv \frac{W_w - W_d}{W_w} \times 100 \tag{2}$$

Moreover, the totality porosity ($\varepsilon$) of membranes was calculated by Eq. (3):

$$\varepsilon(\%) \equiv \frac{W_w - W_d}{\rho_f V_m} \times 100 \tag{3}$$

where $W_d$, $W_w$, $V_m$, and $\rho_f$ are the dry, wet membranes weight (g), membrane volume (cm$^3$), and water density (g/cm$^3$), respectively.

For calculation, mean pore size of membranes ($r_m$), the equation of Guerout-Elford-Ferry was used:

$$r_m \equiv \sqrt{\frac{(2.9 - 1.75\varepsilon)8\eta LQ}{\varepsilon A \Delta p}} \tag{4}$$

where L is the membrane thickness (m), A is the membrane filtration locality (m$^2$), and $\varepsilon$ is the membrane porosity. $\eta$, ΔP, and Q are the water viscosity ($8.9\times10^{-4}$ Pa·s), operating pressure (0.45 MPa) and the volume of the permeated unalloyed water flux (m$^3$/s), respectively.

**5. Membrane Filtration Proficiency Analysis**

The prepared membrane proficiency was determined by a filtration system (set up a stalemate cell per an impressive membrane locality of 11.94 cm$^2$) in pressure of 4.5 bar, as shown in Fig. 1. Aqueous solutions of $Na_2SO_4$ with concentration (1,000 g/L), $CrSO_4$, $Pb(NO_3)_2$, and $Cu(NO_3)_2$ with the concentration of 500 g/L were used as feed solutions. The following equations were utilized for the computation of the rejection (R) permeation flux ($J_{w,1}$) and permeation flux ($J_{w,1}$):

$$J_{w,1} \equiv \frac{V}{A \times t} \tag{5}$$

$$R(\%) \equiv \frac{C_f - C_p}{C_f} \times 100 \tag{6}$$

where Δt, $C_p$, $C_f$, A and V are sampling time (h), ion concentration in permeate and feed, membrane area (m$^2$), volume of permeated

**Table 1. The compilation of casting solution used to prepare the membrane**

| Membrane | $Cu_2O$ (wt%) | PVP (wt%) | PES (wt%) | DMAc (wt%) |
|---|---|---|---|---|
| M0 | 0 | 1 | 18 | 81 |
| M1 | 0.05 | 1 | 18 | 80.95 |
| M2 | 0.1 | 1 | 18 | 80.9 |
| M3 | 0.5 | 1 | 18 | 80.5 |
| M4 | 1 | 1 | 18 | 80 |
| M5 | 2 | 1 | 18 | 79 |

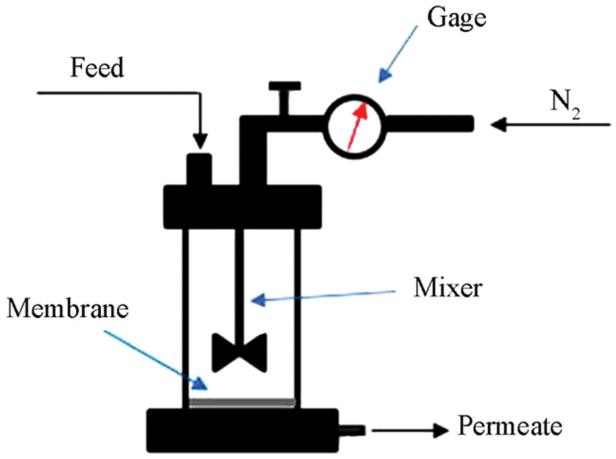


**Fig. 1. Schematic diagram of used filtration system.**

flux (L), respectively.

The fouled membranes kept in water for 1 h. The flux of unalloyed water ($J_{w,2}$ ($L/m^2h$)) was measured afresh at 0.45 MPa for 1 h for determining the amount of flux recovery ratio (FRR%). The FRR% was determined for the antifouling capability of membranes as follows:

$$FRR(\%) \equiv \frac{J_{w,1}}{J_{w,2}} \times 100 \quad (7)$$

## RESULTS AND DISCUSSION

### 1. Characterizations of Nanoparticles

Fig. 2(a) shows FTIR analysis of synthetic $Cu_2O$ nanoparticles at around 500-4,000 $cm^{-1}$. The climaxes in the ambit of 3,444.15 illustrate O-H stretching fluctuations and the bending mode, respectively. Furthermore, bands in the range of 828.07 and 621.35 $cm^{-1}$ represent the O-Cu-O and Cu-O, Cu-O-Cu stretching fluctuations [41,42].

Fig. 3 shows FESEM representations of synthesized nanoparticles. The FESEM micrographs determined nanoparticle size. The results confirmed the high quality of nanoparticles without any type of impurity. The XRD schema of the synthesized powder samples is shown in Fig. 4. Morphology and the quantity of crystals were characterized by XRD analysis. Also, the crystallite size of prepared $Cu_2O$ nanoparticles was obtained at 21.46 nm using Debye Scherrer equation (Eq. (1)). The configuration of nanoparticles plays a pivotal role in determining their quality. Many nanostructures come in the form of cubes, polygons, octagons, spheres, and so on. As the shred size decreases, the surface-to-volume ratio enlarges and the shape can affect the surface structure [46].

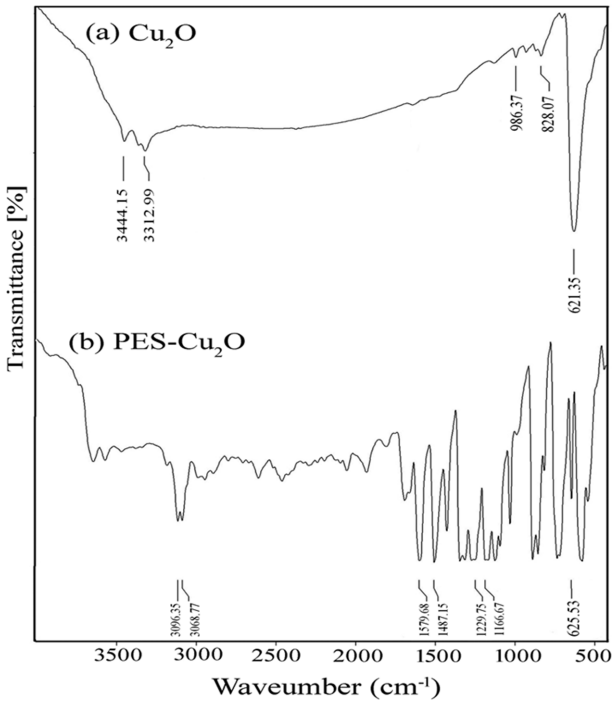


**Fig. 2. FTIR spectrum of (a) $Cu_2O$ nanoparticles; (b) PES/$Cu_2O$ membrane.**

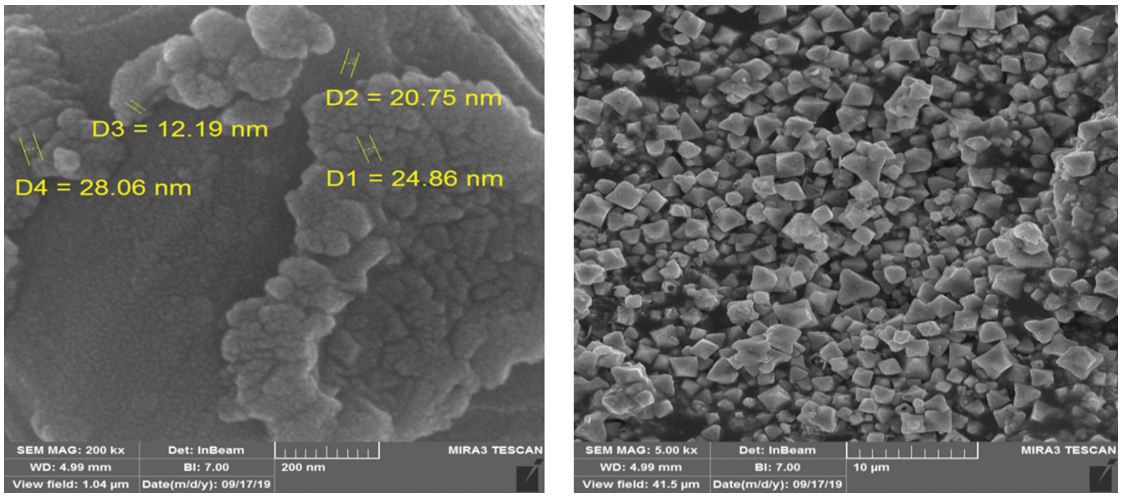


**Fig. 3. FESEM images of $Cu_2O$ nanoparticles.**

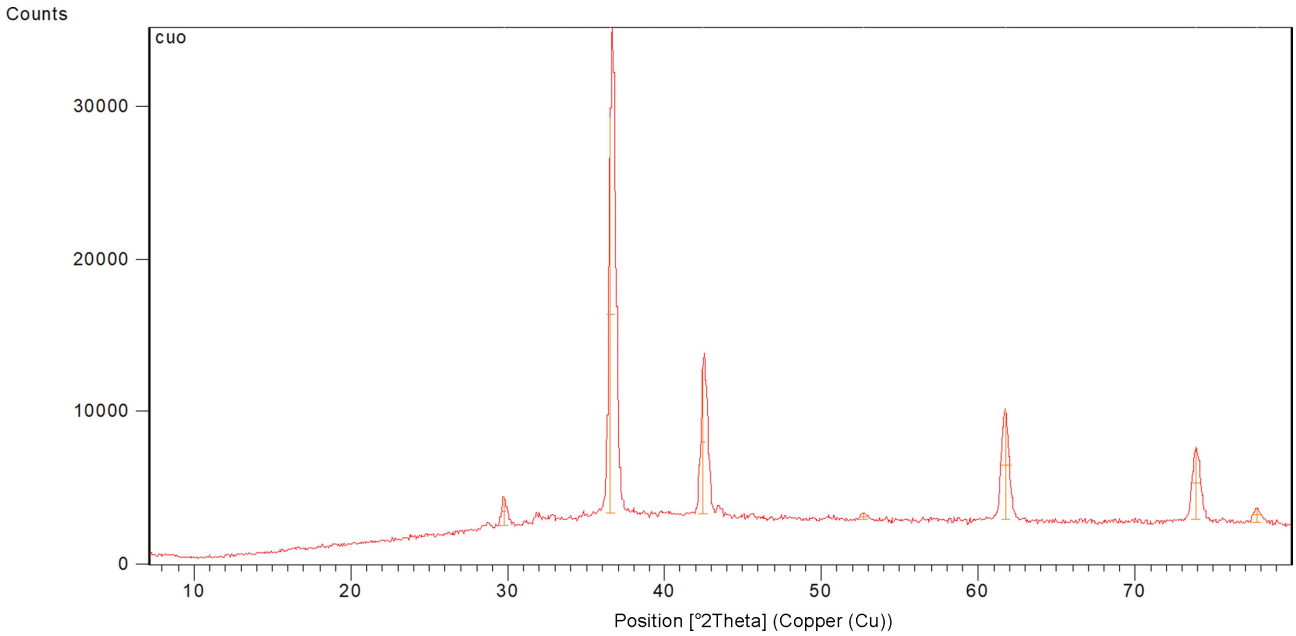


**Fig. 4. X-ray diffraction (XRD) arrangement of $Cu_2O$ nanoparticles.**

## 2. Characterizations of Membrane

### 2-1. FTIR Analyses

FTIR analysis of PES blend membranes is shown in Fig. 2(b). Peaks at 1,229.75 and 1,166.67 $cm^{-1}$ indicate the asymmetric and symmetric stretching fluctuation of S=O bonds, respectively [47]. The climaxes in the range of 1,487.15-1,579.68 $cm^{-1}$ were noticed for benzene ring stretching [48]. The synthesized nanoparticles and membrane exhibited a broad absorption peak around 3,068.77, 3,096.35 $cm^{-1}$ regarding extension of hydroxyl functional groups (-O-H) that was obtained via the addition of $Cu_2O$ [49].

### 2-2. Membrane Morphology

The images of FESEM in Fig. 5 show cross-sectional vignettes of gathered NF membranes with distinct values of the $Cu_2O$ nanoparticles. Images show asymmetric and porous structures for all membranes containing a dense thin selective layer and a spongy bulky sub-layer as support with finger-like structure including micro-voids. Macro-voids form by increasing nanoparticle values in the membrane in the outcome of the phase inversion process and faster mass exchange among water (non-solvent) and DMAC (solvent). Thus, more significant voids and channels are produced in the spongy-like structure [5]. But in high values of nanoparticles, the micro-voids and channels size decrease due to aggregation of nanoparticles and increased solution viscosity [5,13,50].

With the attendance of these nanoparticles in the membrane constitution during the membrane fabrication process, the rate of infiltration of the non-solvent current in the polymer film and solvent outflow increases, thus increasing the rate of phase separation. As a result, the solvent is removed more rapidly from the polymer film; the upper active layer of the membrane is rapidly formed, resulting in additional durability to mass transfer, thereby incrementing the exchange time between the non-solvent and the solvent in the substrate. For this reason, the cavities in the substrate become spongy to finger-like. This creates cavities in the membrane structure and increases porosity. According to Fig. 5, the membrane without the nanoparticles is spongier than other membranes and passes less water flux. By adding 0.05 wt% nanoparticles, the membrane structure is close to the finger state and larger cavities are created in the membrane structure. The porosity of the substrate increased slightly compared with the genuine membrane (see Table 2), which may be owing to the low amount of nanoparticles that did not affect the phase separation process and the rate of solvent exit from the polymer film. Increasing the active layer thickness and porosity in the substrate is clear in 0.1 wt% nanoparticles in the polymer solution. With adding nanoparticles, larger and longer cavities have emerged in the membrane structure. The cavity size was increased by adding nanoparticles concentration at 0.5 wt% (see Table 2). By increasing concentrations of nanoparticles in the M4 and M5 membranes, the size of the cavities decreased, which could be due to the aggregation and accumulation of nanoparticles on the surface of the membrane and the non-uniform dispersal of the nanoparticles in the polymer solution. These phenomena can occur in the ultrasonic bath and/or the nanoparticle movement toward the surface of the membrane amid the phase change procedure. Thus, numerous amounts of nanoparticles lead to a decrease in the transport pathways and filling of the cavities, which have negatively affected

**Table 2. Median pore size and porosity of the fabricated membranes**

| Membrane | Mean pore size (m) | Porosity (%) |
|---|---|---|
| M0 | 3.938E-09 | 60.96 |
| M1 | 8.372E-09 | 54.0709 |
| M2 | 6.0276E-09 | 70.98 |
| M3 | 4.454E-09 | 67.85 |
| M4 | 8.993E-10 | 78.079 |
| M5 | 9.2784E-10 | 72.44 |

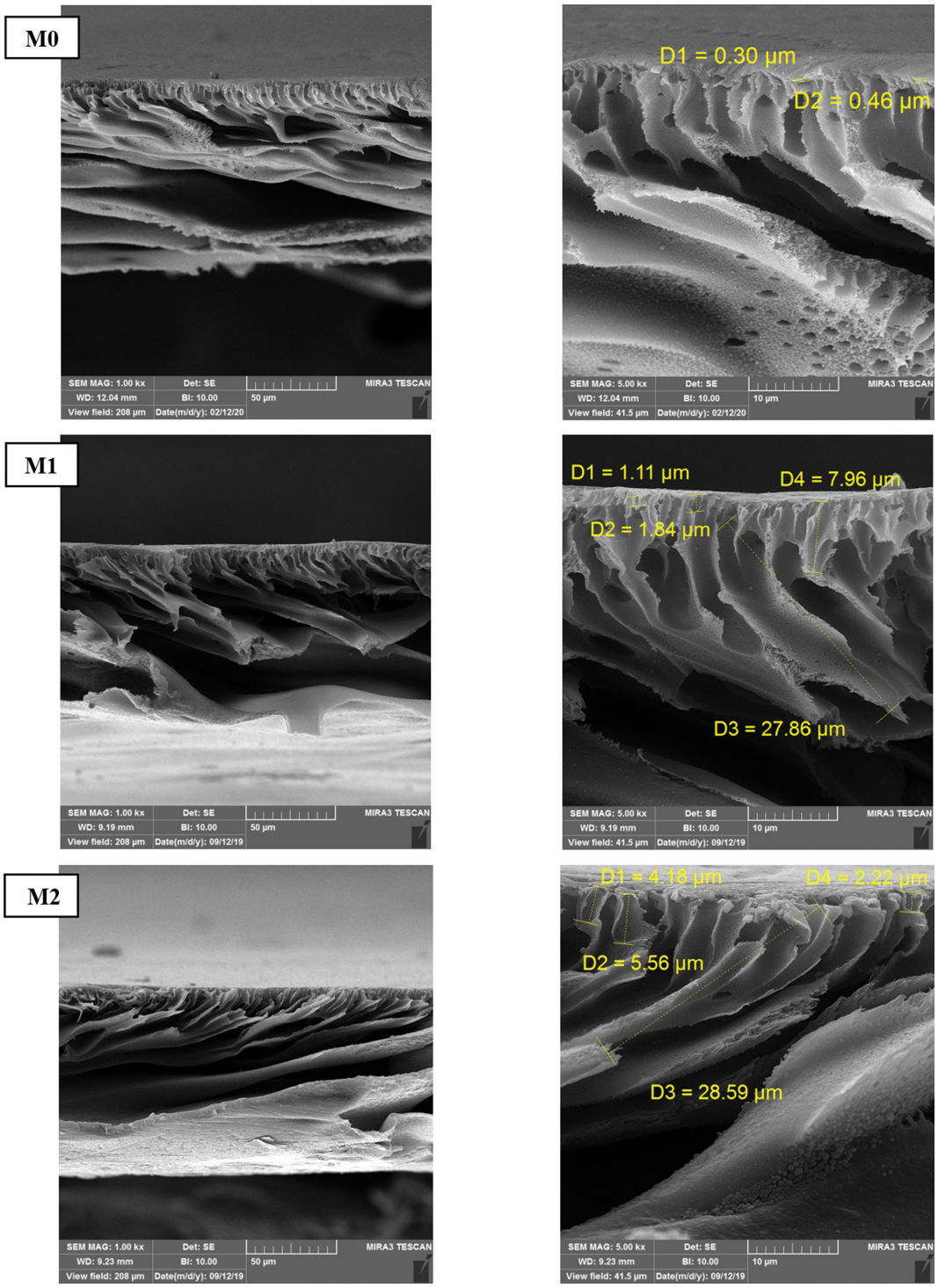


**Fig. 5. Images FESEM from fabricated membranes.**

the membrane flux. Moreover, the reduction in porosity in M3 and M5 membranes could be due to the accumulation of nanoparticles and their low dispersion at high concentrations.

Also, 3D surface images by SPM software (version 6.4, Femtoscan) were used for the investigation of surface morphology and measuring membrane roughness. Three-dimensional surface images are indicated in Fig. 6 for the membranes with a scanning area of 6 µm×6 µm. The roughness of membranes is explained in terms of the median root square of the height data ($R_q$) and the median roughness ($R_a$), maximum roughness ($R_{max}$). Computed roughness parameters of the arranged membranes are in Table 3. According to Table 3, via increment of the value of nanoparticles in the membrane matrix, the surface roughness of the membrane decreased from 4.628 nm for the bare PES membrane to 3.023 nm for the

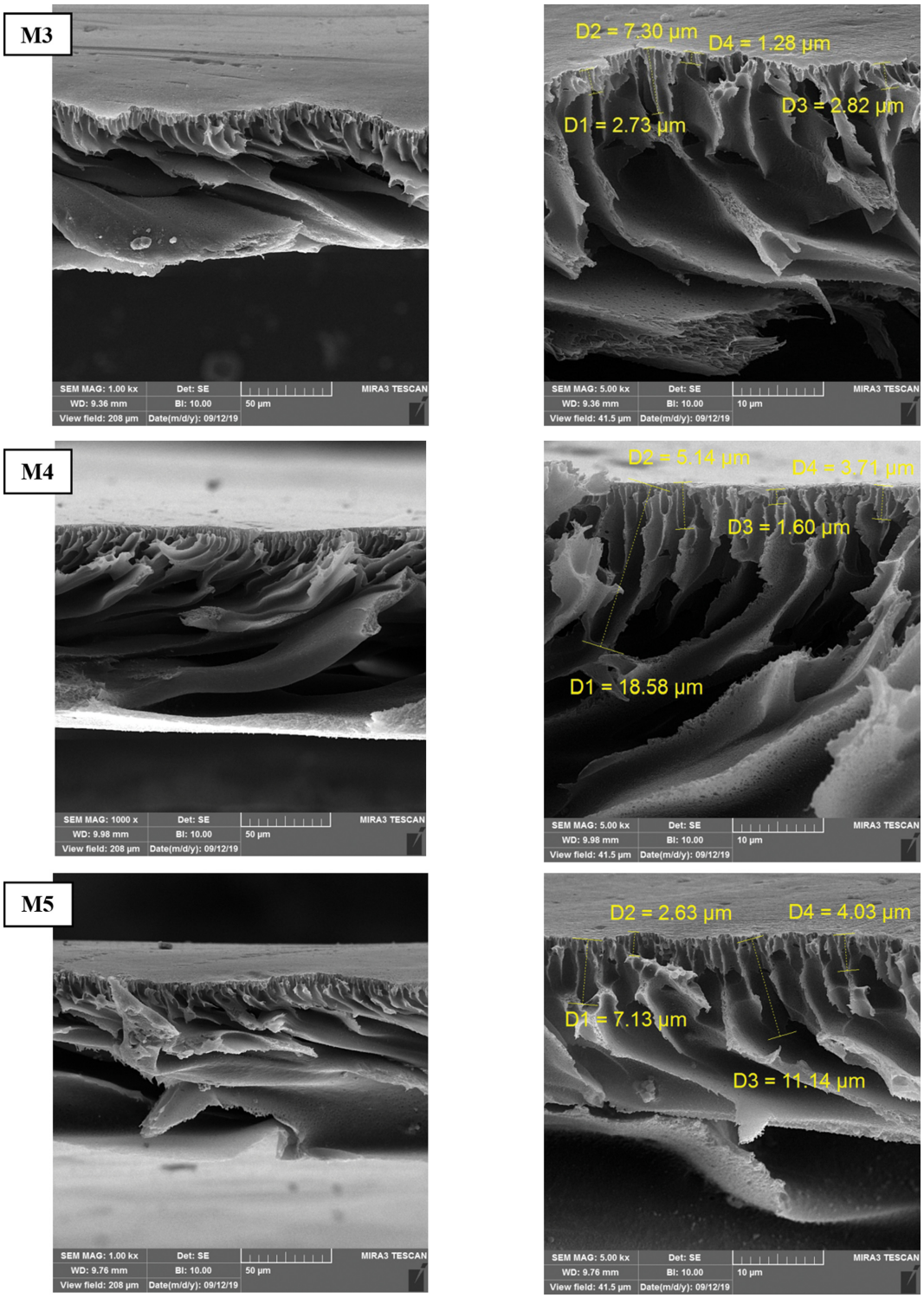


**Fig. 5. Continued.**

mixture membrane at 2 wt% of nanoparticles [51,52]. This can be owing to the stuffing of pores and valleys with nanoparticles on the surface of the membrane and then the reduction of pore sizes [53,54]. In M2 and M5, the average roughness increased to 4.489 and 3.023 nm, again due to the aggregation of nanoparticles on the membrane surface by unsuitable dispersion [49,55-57]. In M4 the high porosity and uniform repartition of nanoparticles on the surface is such that the nanoparticles fill the surface cavities and make the surface smoother.

## 3. Filtration Performance

### 3-1. Contact Angle and Water Content

Fig. 7(a) shows the contact angle for the mixture and bare mem-

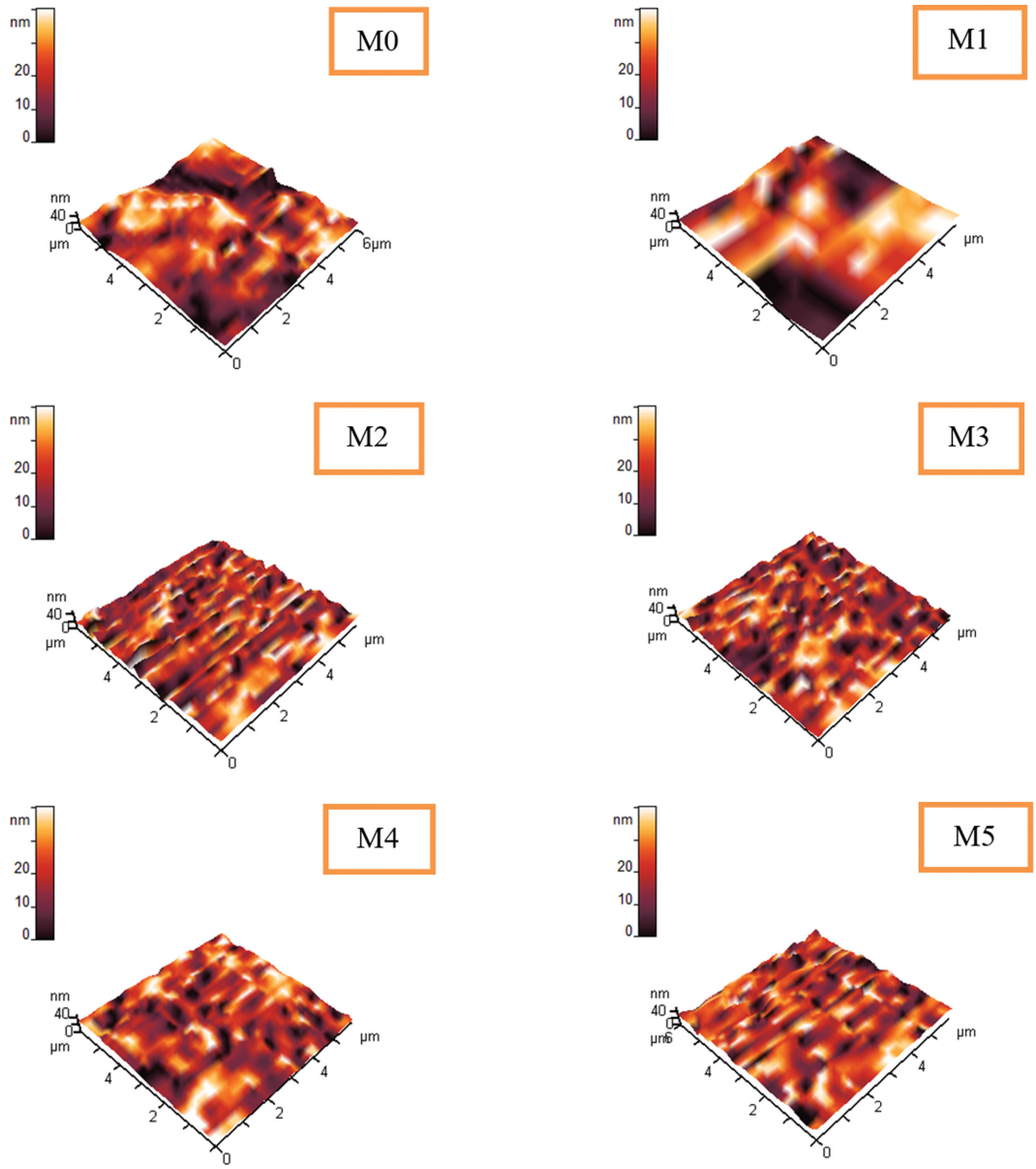


**Fig. 6. Surface AFM representations of the bare and blended membranes.**

**Table 3. The surface roughness parameters of the arranged membranes**

| Membrane | $R_a$ (nm) | $R_q$ (nm) | $R_{max}$ (nm) |
|---|---|---|---|
| M0 | 4.628 | 5.594 | 23.8 |
| M1 | 4.261 | 5.076 | 16.9 |
| M2 | 4.489 | 5.773 | 27.16 |
| M3 | 3.782 | 4.545 | 18.46 |
| M4 | 2.352 | 3.021 | 13.61 |
| M5 | 3.023 | 4.047 | 20.71 |

branes. Membrane hydrophilicity is indicated via measurement of the water contact angle. The contact angle is among smooth straight surface and water glob. The membrane with an inferior contact angle is more hydrophilic. From Fig. 7, it is clear that incorporating $Cu_2O$ nanoparticles into the membrane matrix enhances membrane hydrophilicity. Because adding $Cu_2O$ nanoparticles increases OH functional groups, which increases membrane hydrophilicity. With increasing nanoparticle concentration, the water contact angle decreased from 62° for the bare membrane to 30° for the mixture membrane. Improving hydrophilicity can be a result of hydroxyl functional groups in nanoparticles, which leads to easy transport of water molecules by hydrogen bonding among hydroxyl groups and water molecules [5,49,58,59].

Water content is indicative of hydrophilicity rate and membrane swelling. Fig. 7(b) shows the measured water content of the arranged membranes. The results show that the modified membranes per $Cu_2O$ nanoparticles have higher water content than pure PES membrane. The hydrophilicity of copper oxide (I) nanoparticles, which

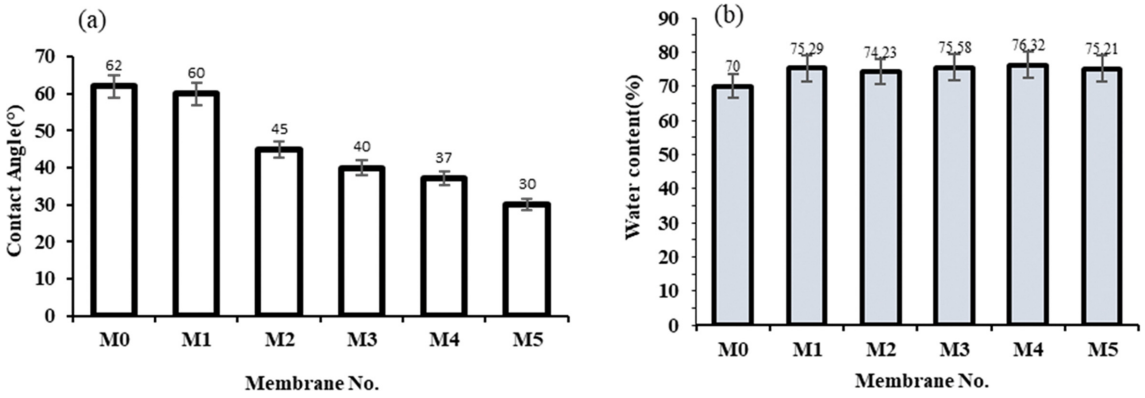


**Fig. 7. (a) Contact angle and (b) water content of arranged membranes at different concentrations of nanoparticles.**

causes hydrogen bonding between the nanoparticles and water, as well as the increase in pores size and the substrate porosity can be the reasons for the increase in membrane hydrophilicity. As the membrane absorbs water, it swells and the pore size of the membrane increases [52,60,61]. The amount of stored water content in the M2 and M5 membranes decreased, possibly due to the filling and blockage of transverse channels with a high volume of nanoparticles in the cavities and the formation of smaller cavities [56, 57,65,66].

3-2. Pure Water Flux

Fig. 8 represents the pure water (PWF) of the fabricated membranes. The highest PWF (36.78 L/m$^2$h) was observed for M1. From the comparison between the bare and blended PES membranes, it is clear that the median pore size of membrane increased with increasing nanoparticles and led to a sharply increase in PWF [5,62-64]. A bigger average membrane pore size was obtained owing to the adsorption of water molecules into the membrane structure by hydrophilic functional groups (-OH) in nanoparticles and increased free volume pending the phase inversion process [65-67]. Nonetheless, the porosity of membranes increased by increasing nanoparticle concentration, but decreasing PWF is attributed to decreasing mean pore size in a high concentration of hydrophilicity $Cu_2O$ nanoparticles into blended membrane matrix and pore blockage. Also,

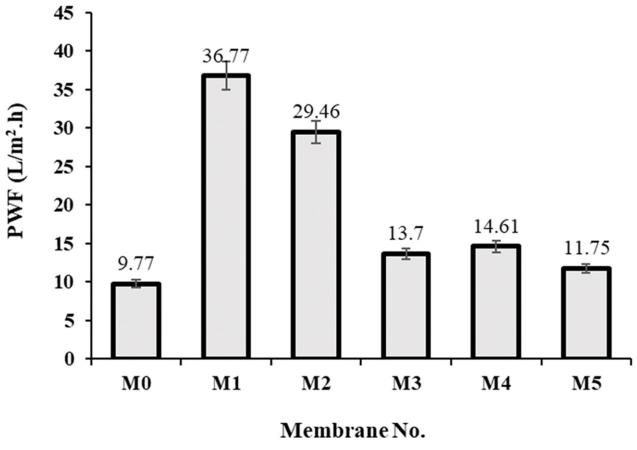


**Fig. 8. The pure water flux (PWF) of the fabricated membranes.**

interconnects channel formation (as shown in FESEM images) in the structure can reduce PWF [60,68-70]. The connection and dimensions of pores and their shape affect ionic or molecular transfer behavior. In general, regular and connected 3D pores are preferred for applications. Because, closed cavities have no role in adsorption and diffusion, in structure can reduce PWF. The nanoparticle agglomeration in a great concentration of nanoparticles and the decline of mean pore size reduces the efficient sites of nanoparticles [71-73].

3-3. Salt Rejection

The flux and salt rejection are the most essential features in determining membrane performance. From salt solutions $Na_2SO_4$, $Pb(NO_3)_2$, $CrSO_4$, and $Cu(NO_3)_2$ were used to investigate the separation efficiency of the arranged membranes. Data of salt water flux and rejection are provided in Fig. 9(a), (b), (c), and (d).

The results show the highest rejection of $Na_2SO_4$, $CrSO_4$, $Pb(NO_3)_2$, $Cu(NO_3)_2$ salt solutions for the mixture membrane containing 2 wt% of $Cu_2O$, which were 66.94%, 79.38%, 85.08%, and 81% respectively, whereas they measured 45.87%, 45%, 46% and 49% for the bare membrane. According to Fig. 9(a), the $Na_2SO_4$ rejection was reduced primarily from 45.87% in M0 to 45% in M1 owing to increased average pore size and porosity that led to the crossing of salt ions. When the membrane absorbs water and swells, the size of the pores increases due to the capillary suction of the liquid and solution; this occurrence causes a weak rejection of small salts and salts [60]. But high concentrations of $Cu_2O$ nanoparticles increased $Na_2SO_4$ rejection, which can be caused by a sharply decreasing mean pore size. Also, another main reason is the effect of Donnan exclusion on salt ion rejection. Thus, hydroxyl groups with negative charges in membrane structure repulse negative ions ($SO_4^{2-}$) of salt molecules that enhance by the increase of nanoparticle ratios.

The adsorption of $Cr^{2+}$ molecule by negative nanoparticles in the hydrophilic surface of the blended membranes is a significant factor for $CrSO_4$ rejection. The $Cr^{2+}$ rejection boosted from 45% for the bare membrane to 79.38% for M5. $CrSO_4$ rejection decreased from 78.48% for M1 to 77.34% for M4 due to porosity increase of blended membranes (see Fig. 9(b)). Also, other reasons are finger-like structure, the constitution of continuous channels, and more holes in the membrane matrix. The reduction in selective layer thick-

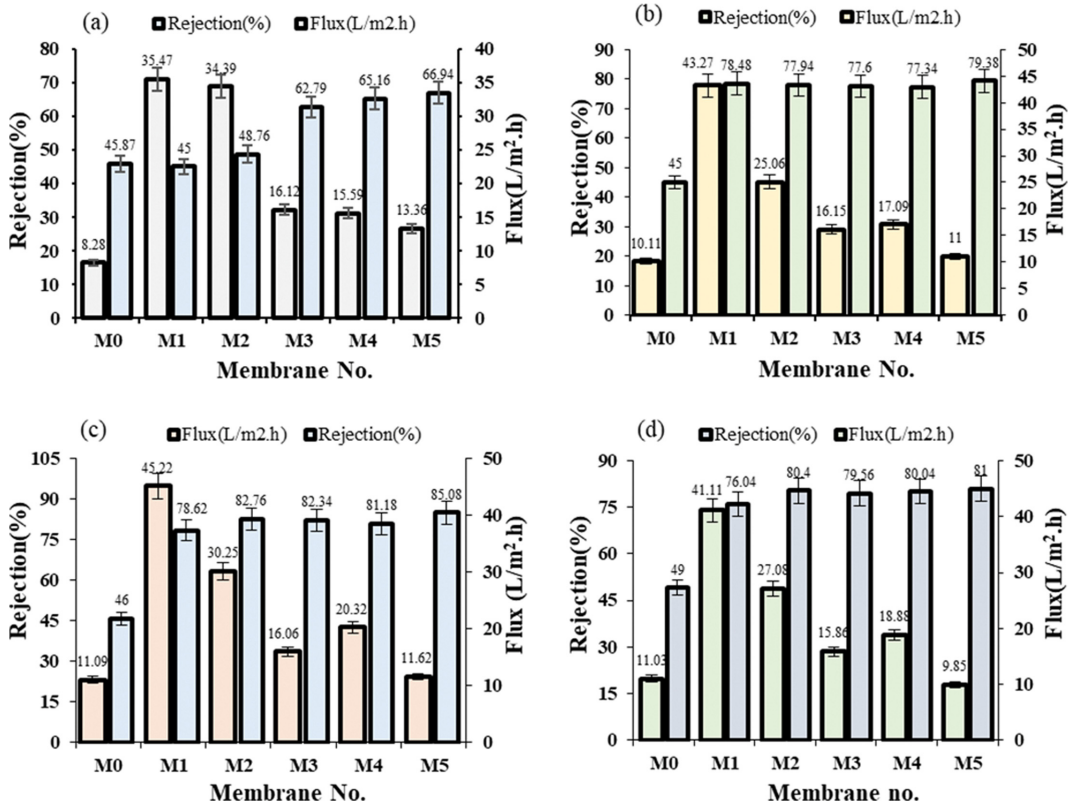


**Fig. 9. Flux and rejection of different salt solution: (a) $Na_2SO_4$, (b) $CrSO_4$, (c) $Pb(NO_3)_2$ and (d) $Cu(NO_3)_2$.**

ness (see Fig. 5) led to reduced membrane resistance against ion transport.

Fig. 9(c) and Fig. 9(d) characterize the rejection of $Pb(NO_3)_2$ and $Cu(NO_3)_2$ solutions. The most important factor in increasing rejection is the adsorption mechanism induced by saturation of membrane adsorption sites by adsorbed $Pb^{2+}$ and $Cu^{2+}$ metal ions on the membrane surface, and its consequences are in the rejection of these ions. The rejection of copper increased from 49% in the bare PES to 81% in M5 and leads rejection increased from 46% in M0 to 85.08% in M5 due to increment of adsorption sites by adsorption behavior of nanoparticles and electrostatic exclusion of $NO_3^-$ ions by formed negative charges by hydroxyl groups. The decreasing rejection of heavy metal ions in M1 can be owing to great PWF and crossing of metal ions by water molecules. The hydrated radius for $Cu^{2+}$ ions is higher than $Pb^{2+}$ and has better repulsion of $NO_3^-$ ions in comparison with $Pb^{2+}$. The slight reduction in onerous metal ion rejection for membranes of M2 to M4 can be due to enhancing porosity of membrane and aggregation of nanoparticles in great concentration that decreases the efficacious surface of nanoparticles concomitant with the accessible adsorption sites. Finally, it increased in M5 due to tighter pores in the membranes.

The high porosity of the M3 and M4 membranes is a reason for the slight decrease in metal ion rejection. The increase in the flux of the M4 membrane is also a result of this change in its structure. The M5 membrane had the highest rejection of heavy metal solutions, which could be due to the decrease in the size of the pores and their closing by metal ions and the increased thickness of the separator layer.

## 4. Antifouling Properties of the Membranes

Flux recovery ratio (FRR%) of the fabricated membranes is shown in Fig. 10. FRR% determines the membrane recycling potential after salt fouling. The membrane fouling can reduce the lifetime, permeation flux and selectivity, which are considered as an important problem. The M1 membrane due to its larger cavities and M4 due to its high porosity in its structure exhibited better antifouling properties than other membranes. The lowest flux recovery value is related to M5, which has the lowest cavity size and surface roughness than other membranes, which could be owing to the collec-

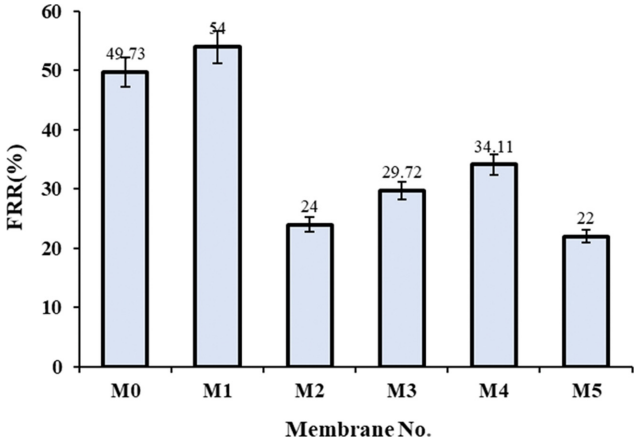


**Fig. 10. Flux recovery ratio (FRR%) of the fabricated membranes.**

tion of high concentrations of nanoparticles on the surface and inside the membrane. The decrease in FRR% for membranes may be due to the agglomeration of nanoparticles, which diminishes the efficacious surface of nanoparticles also can be the consequence of reduced selective layer thickness and interconnect channels into membrane construction. It means that the salt ions were ensnared into the channels and could not pull out of channels because of the confrontation with closed directions. Higher FRR% value shows an excelling antifouling manner for the membrane M1.

## CONCLUSION

Cuprous oxide nanoparticles ($Cu_2O$) were synthesized by electrochemical methods. Then the various concentrations of synthesized nanoparticles were used to fabricate PES NF membranes by the phase inversion procedure. Synthesized nanoparticles and membranes were characterized by FTIR, FESEM, XRD analyses and 3D surface images. The presence of $Cu_2O$ nanoparticles caused a momentous enlargement in the flux of unalloyed water due to the attendance of hydrophilic groups and an enlargement in the median pore size and porosity of membranes. Modified membranes showed smoother surface than the pure PES membranes. The $Na_2SO_4$, $CrSO_4$, $Cu(NO_3)_2$ and $Pb(NO_3)_2$ rejection reached 66.94%, 79.38%, 81% and 85.08% for M5 membrane, which was considerably higher than the bare PES membrane. Moreover, the antifouling properties of the membranes were enhanced by decreasing surface roughness and increasing hydrophilic groups.

## REFERENCES


1. S. Yu, M. Ma, J. Liu, J. Tao, M. Liu and C. Gao, *J. Membr. Sci.*, **379**, 164 (2011).
2. S. Bandehali, A. Moghadassi, F. Parvizian, Y. Zhang, S. Mohsen Hosseini and J. Shen, *Sep. Purif. Technol.*, **242**, 116745 (2020).
3. F. Parvizian, F. Ansari and S. Bandehali, *Chem. Eng. Res. Des.*, **156**, 433 (2020).
4. S. Hosseini, S. Amini, A. Khodabakhshi, E. Bagheripour and B. Van der Bruggen, *J. Taiwan Inst. Chem. Eng.*, **82**, 169 (2018).
5. S. Bandehali, A. Moghadassi, F. Parvizian and S. Hosseini, *Korean J. Chem. Eng.*, **36**, 1657 (2019).
6. S. Bandehali, A. Moghadassi, F. Parvizian, S. M. Hosseini, T. Matsuura and E. Joudaki, *J. Energy Chem.*, **46**, 30 (2020).
7. M. Maarefian, S. Bandehali, S. Azami, H. Sanaeepur and A. Moghadassi, *Int. J. Energy Chem.*, **43**, 8217 (2019).
8. H. Sanaeepur, A. E. Amooghin, S. Bandehali, A. Moghadassi, T. Matsuura and B. Van der Bruggen, *Prog. Polym. Sci.*, **91**, 80 (2019).
9. B. Van der Bruggen and C. Vandecasteele, *Environ. Pollut.*, **122**, 435 (2003).
10. S. Bandehali, A. Moghadassi, F. Parvizian, J. Shen and S. Hosseini, *Korean J. Chem. Eng.*, **37**, 263 (2020).
11. S. Bandehali, F. Parvizian, A. R. Moghadassi and S. M. Hosseini, *J. Polym. Res.*, **26**, 211 (2019).
12. E. Staude, *Marcel Mulder: Basic principles of membrane technology*, Kluwer Academic Publishers, Dordrecht, Boston, London (1991).
13. S. Bandehali, F. Parvizian, A. Moghadassi and S. M. Hosseini, *Sep. Purif. Technol.*, **237**, 116361 (2019).
14. S. M. Hosseini, M. Afshari, A. R. Fazlali, S. Koudzari Farahani, S. Bandehali, B. Van der Bruggen and E. Bagheripour, *Chem. Eng. Res. Des.*, **147**, 390 (2019).
15. E. Bagheripour, A. Moghadassi and S. M. Hosseini, *Int. J. Eng.*, **30**, 821 (2017).
16. D. Laha, A. Pramanik, A. Laskar, M. Jana, P. Pramanik and P. Karmakar, *Mater. Res. Bull.*, **59**, 185 (2014).
17. J. Kim, A. Sotto, J. Chang, D. Nam, A. Boromand and B. Van der Bruggen, *Micropor. Mesopor. Mater.*, **173**, 121 (2013).
18. N. Maximous, G. Nakhla, K. Wong and W. Wan, *Sep. Purif. Technol.*, **73**, 294 (2010).
19. H. Sanaeepur, A. Ebadi Amooghin and S. Bandehali, LAP LAMBERT Academic Publishing, Beau Bassin, Mauritius (2018).
20. P. A. Korzhavyi and B. Johansson, Swedish Nuclear Fuel and Waste Management Co. (2011).
21. H. R. Ghorbani, *Oriental J. Chem.*, **30**, 803 (2014).
22. S. S. Sawant, A. D. Bhagwat and C. M. Mahajan, *J. Nano-And Electron Phys.*, **8**, 010351 (2016).
23. N. Topnani, S. Kushwaha and T. Athar, *Int. J. Green Nanotechnol.: Mater. Sci. Eng.*, **1**, M67 (2010).
24. H. W. Richardson, CRC Press (1997).
25. S. Saeednia, P. Iranmanesh, M. Hatefi Ardakani and S. Sinaei, *Nanostructures*, **5**, 297 (2015).
26. H. Yang, J. Ouyang, A. Tang, Y. Xiao, X. Li, X. Dong and Y. Yu, *Mater. Res. Bulletin*, **41**, 1310 (2006).
27. R. V. Kumar, Y. Mastai, Y. Diamant and A. Gedanken, *J. Mater. Chem.*, **11**, 1209 (2001).
28. N. Zhang, Y. Du, Y. Zhang and C. Wang, *J. Mater. Chem.*, **21**, 5408 (2011).
29. X. Guo, W. Lv and X.-Y. Li, *J. Phys. Chem. C*, **118**, 11062 (2014).
30. A. Musa, T. Akomolafe and M. Carter, *Sol. Energy Mater. Sol. Cells*, **51**, 305 (1998).
31. M. Kouti and L. Matouri, *IEEE Trans Nanotechnol.*, **17**, 73 (2010).
32. M. Valodkar, A. Pal and S. Thakore, *J. Alloys Compd.*, **509**, 523 (2011).
33. H. K. Khattar, S. W. R. Al-Hasnawi and F. A. Al-Saady, *Int. J. Electrical Computer Sci. IJECS-IJENS*, **15**, 6 (2015).
34. M. Figueroa, R. Gana, W. Cooper and J. Ji, *J. Appl. Electrochem.*, **23**, 308 (1993).
35. F. Xu, M. Deng, G. Li, S. Chen and L. Wang, *Electrochim. Acta*, **88**, 59 (2013).
36. M. J. Siegfried and K.-S. Choi, *Angew. Chem. Int. Ed.*, **44**, 3218 (2005).
37. L. Rodríguez-Sánchez, M. C. Blanco and M. A. López-Quintela, *J. Phys. Chem. B*, **104**, 9683 (2000).
38. K. Borgohain, N. Murase and S. Mahamuni, *J. Appl. Phys.*, **92**, 1292 (2002).
39. A. García, B. Rodríguez, D. Oztürk, M. Rosales, D. Diaz and A. Mautner, *Polym. Bull.*, **75**, 2053 (2018).
40. F. Zareei and S. M. Hosseini, *Sep. Purif. Technol.*, **226**, 48 (2019).
41. R. Singh, V. Yadav and M. K. Purkait, *Sep. Purif. Technol.*, **212**, 191 (2019).
42. Z. Xu, S. Ye, G. Zhang, W. Li, C. Gao, C. Shen and Q. J. J. o. m. s. Meng, *J. Membr. Sci.*, **509**, 83 (2016).
43. N. Nasrollahi, V. Vatanpour, S. Aber, N. M. J. S. Mahmoodi and P. Technology, *Sep. Purif. Technol.*, **192**, 369 (2018).

44. P. Roy Choudhury, S. Majumdar, G. C. Sahoo, S. Saha and P. Mondal, *J. Chem. Eng.*, **336**, 570 (2018).
45. S. Hosseini, E. Jashni, M. Habibi, M. Nemati and B. Van der Bruggen, *J. Membr. Sci.*, **541**, 641 (2017).
46. J. Hwang, A. Ejsmont, R. Freund, J. Goscianska, B. V. Schmidt and S. Wuttke, *Chem. Soc. Rev.*, **49**, 3348 (2020).
47. N. Nasrollahi, V. Vatanpour and S. Aber, *J. Water Process. Eng.*, **31**, 100891 (2019).
48. H. Abdul Mannan, H. Mukhtar, M. Shima Shaharun, M. Roslee Othman and T. Murugesan, *J. Appl. Polym. Sci.*, **133** (2016).
49. N. Nasrollahi, S. Aber, V. Vatanpour and N. M. Mahmoodi, *Mater. Chem. Phys.*, **222**, 338 (2019).
50. E. Bagheripour, A. Moghadassi, S. Hosseini, B. Van der Bruggen and F. Parvizian, *J. Ind. Eng. Chem.*, **62**, 311 (2018).
51. M. Rahimi, S. Dadari, S. Zeinaddini and E. J. Mohamadian, *Korean J. Chem. Eng.*, **34**, 1444 (2017).
52. N. Ghaemi, S. S. Madaeni, P. Daraei, H. Rajabi, T. Shojaeimehr, F. Rahimpour and B. Shirvani, *J. Hazard. Mater.*, **298**, 111 (2015).
53. H.-Z. Zhang, Z.-L. Xu, H. Ding and Y.-J. Tang, *Desalination*, **420**, 158 (2017).
54. S. Dadari, M. Rahimi and S. Zinadini, *Korean J. Chem. Eng.*, In press (2022).
55. E. Bagheripour, A. Moghadassi, S. Hosseini, M. Ray, F. Parvizian and B. Van der Bruggen, *Chem. Eng. Res. Des.*, **132**, 812 (2018).
56. A. Razmjou, J. Mansouri and V. Chen, *J. Membr. Sci.*, **378**, 73 (2011).
57. M. Peyravi, A. Rahimpour, M. Jahanshahi, A. Javadi and A. Shockravi, *Micropor. Mesopor. Mater.*, **160**, 114 (2012).
58. S. Dadari, M. Rahimi and S. Zinadini, *J. Chem. Eng.*, **431**, 134116 (2022).
59. S. Dadari, M. Rahimi and S. J. Zinadini, *Desalination*, **377**, 34 (2016).
60. P. Su, F. Wang, Z. Li, C. Y. Tang and W. Li, *J. Mater. Chem. A*, **8**, 15319 (2020).
61. G. Moradi, S. Zinadini, L. Rajabi and S. J. Dadari, *Appl. Surf. Sci.*, **427**, 830 (2018).
62. S. M. Hosseini, F. Moradi, S. K. Farahani, S. Bandehali, F. Parvizian, M. Ebrahimi and J. Shen, *Mater. Chem. Phys.*, **269**, 124720 (2021).
63. F. Zareei, S. Bandehali and S. M. Hosseini, *Korean J. Chem. Eng.*, **38**, 1014 (2021).
64. S. Bandehali, F. Parvizian, H. Ruan, A. Moghadassi, J. Shen, A. Figoli, A. S. Adeleye, N. Hilal, T. Matsuura, E. Drioli and S. M. Hosseini, *J. Ind. Eng. Chem.*, **101**, 78 (2021).
65. N. Ghaemi, S. S. Madaeni, A. Alizadeh, H. Rajabi and P. Daraei, *J. Membr. Sci.*, **382**, 135 (2011).
66. H. M. Hegab and L. Zou, *J. Membr. Sci.*, **484**, 95 (2015).
67. S. M. Hosseini, M. S. Banijamali, S. K. Farahani and S. Bandehali, *Korean J. Chem. Eng.*, In press (2022).
68. A. Moghadassi, S. Moradi and S. J. Bandehali, *Korean J. Chem. Eng.*, **37**, 1963 (2020).
69. F. Zareei, S. Bandehali, F. Parvizian, S. Hosseini and J. Shen, *Chem. Eng. Res. Des.*, **169**, 204 (2021).
70. S. Bandehali, H. Sanaeepur, A. E. Amooghin, S. Shirazian and S. Ramakrishna, *Sep. Purif. Technol.*, **269**, 118731 (2021).
71. S. Bandehali, F. Parvizian, A. Moghadassi and S. M. Hosseini, *Nanomaterials for the efficient abatement of wastewater contaminants by means of reverse osmosis and nanofiltration*, B. Bonelli, F. S. Freyria, I. Rossetti, R. Sethi Eds., Elsevier, Netherlands (2020).
72. S. M. Hosseini, F. Karami, S. K. Farahani, S. Bandehali, J. Shen, E. Bagheripour and A. J. Seidypoor, *Korean J. Chem. Eng.*, **37**, 866 (2020).
73. S. Bandehali, F. Parvizian, A. Moghadassi, S. Hosseini and J. J. Shen, *J. Polym. Res.*, **27**, 1 (2020).